J. Phys.: Condens. Matter **11** (1999) 6099–6111. Printed in the UK PII: S0953-8984(99)04238-1

Structure and dynamics of liquid lithium: comparison of *ab initio* molecular dynamics predictions with scattering experiments

J A Anta† and P A Madden

Physical and Theoretical Chemistry Laboratory, Oxford University, South Parks Road, Oxford OX1 3QZ, UK

Received 12 May 1999

Abstract. An application of the orbital-free *ab initio* molecular dynamics (OF-AIMD) method to liquid lithium at 470 K and 725 K is presented. The results are compared with data from scattering experiments—x-ray and neutron diffraction results for the static structure factor and inelastic x-ray measurements of the dynamic structure factor. These comparisons reveal a strong sensitivity of the calculated quantities at low scattering vector to the form of the pseudopotential for Li, and lead to an improvement of the previously suggested method for pseudopotential generation for OF-AIMD. By combining x-ray and neutron diffraction data the ion–electron structure factor may be extracted. OF-AIMD results for this quantity are compared with experiment.

1. Introduction

Molecular dynamics methods have been extensively exploited to obtain static and dynamic properties of simple liquid metals [1–5]. Recently, attention has focused on developing *ab initio* approaches which do not rely on the introduction of inter-particle potentials [6–8]: they are, in principle, free from empirical parameters and transferable to all environments, including mixtures. However, these techniques, which are based in the Kohn–Sham (KS) formulation of density functional theory (DFT) [9], require a huge computational effort and only simulations with a small number of particles have been accomplished. An alternative, cheaper, approach, the so-called orbital-free *ab initio* molecular dynamics method (OF-AIMD) [10], gives correct results for structural and dynamical properties of simple metallic systems [11–14]. Recently the OF-AIMD method has been used to obtain the ion–ion and ion–electron static structure factors of liquid Na, Mg and Al with considerable success [14]. The OF-AIMD technique permits computations with larger samples and longer simulation times, comparable to those routinely used in classical simulations.

Liquid lithium is a system in which the ionic structure and dynamics has been studied thoroughly in recent years [2–4, 15–17]. It exhibits a behaviour that differs markedly from those of the other alkalis [18]. The investigation of this metal at the microscopic level poses significant problems both in the experimental and theoretical fields. The determination of the ionic structure factor from neutron diffraction experiments is not straightforward due to the small atomic mass of the lithium nucleus, which hinders the correction of the data, especially

† Present address: Department of Chemistry, Imperial College of Science, Technology and Medicine, Exhibition Road, London SW7 2AY, UK.

0953-8984/99/326099+13$30.00 © 1999 IOP Publishing Ltd

at low momentum transfers k. X-ray diffraction is not straightforward either because the proportion of valence (delocalized) electrons in Li in comparison with other alkalis is very high and, therefore, corrections due to inelastic Compton scattering are substantial and not totally understood [18, 19]. The dynamic structure factor has been recorded on the recently developed inelastic x-ray instruments [17]. As these authors show, the diffraction and inelastic scattering results present a stringent test for the reliability of computer simulations, especially at low scattering angles. To access this low-wavevector region in simulations, quite large simulation cells are required, bringing the computational advantages of OF-AIMD into play.

From the theoretical point of view, 2s and 2p valence orbitals in Li are very similar in size and energy and can hybridize effectively [1, 20]. This makes non-locality effects very important in Li, hindering the determination of reasonable local pseudopotentials needed to construct inter-particle pair potentials [15]. Despite this, Canales *et al* [4] have achieved a remarkable prediction of a whole set of bulk properties for Li at two different temperatures by using classical molecular dynamics with pair potentials obtained via linear response theory. Also Kresse [2] has calculated the static and dynamic structure factor of Li at 470 K via Kohn–Sham AIMD simulation, with a fully non-local pseudopotential. These new experimental results and simulations provide good benchmarks for evaluating the state of development of the OF-AIMD method, which currently involves a local pseudopotential, especially given the interest in low-wavevector properties and the consequential large simulation cells required.

Finally, Li is an interesting system for which to examine the extraction of ion–electron structure factors from the ratio of x-ray and neutron diffraction measurements [21, 22]. In a previous paper [14], we showed that the theoretically calculated difference between x-ray and neutron diffraction structure factors is considerably smaller than the differences so far measured for Na, Mg and Al, suggesting that it is smaller than intrinsic errors in the experiments. Due to the high ratio of valence to core electrons in Li, the difference between x-ray and neutron diffraction structure factors is expected to be larger than in these other metals. We have therefore calculated the ion–electron structure factor and compared it with data available from experiments [19].

2. Simulation details and pseudopotential generation

A description of the OF-AIMD method has appeared in several previous publications [10–13], together with an evaluation of its computational advantages over a conventional KS-AIMD for metallic systems. Four simulations of liquid Li were performed in the present work, comprising two different thermodynamic states (470 K and 725 K), two different system sizes (176 and 479 particles) and two different pseudopotentials (see below). Details of these simulations can be found in table 1. The average densities were fixed to the experimental values at the chosen temperatures [18]. As seen in table 1, this results in the system being under a small (by simulation standards) positive pressure. A spherical plane-wave cut-off of 18–20 hartrees was introduced to truncate the Fourier expansion of the valence electron density $\rho_e(\boldsymbol{r})$ in all cases.

In all simulations the time step was set equal to 0.5 fs. The samples were equilibrated over 10 000–15 000 steps and in all cases a production run of 20 000 steps was carried out in order to obtain the averaged quantities presented in the following sections. This amounts to a real time of 10 ps. Simulations with the lower number of particles were carried out on a single *Silicon Graphics R10000* 195 MHz processor and required 30–36 seconds of CPU time per step. The simulation with 479 particles was executed in parallel on eight R10000 processors and took 20 seconds of CPU time per simulation step.

As mentioned before, two distinct pseudopotentials have been used to describe Li.

Table 1. Simulation details and properties of liquid Li. The experimental data have been taken from reference [18].

	T/K	N	ρ/kg m^{-3}	P/MPa	$\chi_T/10^{-4}$ MPa^{-1}	c_s/m s^{-1}	D/Å^2 ps^{-1}
OF-AIMD(A)	470	479	513.4	1400	0.98	5300 ± 500	0.82 ± 0.05
OF-AIMD(A)	470	176	513.4	1420	1.41	5600 ± 370	0.79 ± 0.05
OF-AIMD(B)	470	176	513.4	−2600	1.13	4485 ± 370	0.55 ± 0.05
OF-AIMD(A)	725	128	491.0	1380	2.09	5250 ± 340	1.78 ± 0.05
KS-AIMD[a]	470	128	—	—	—	5100 ± 100	0.69
NPA-MD[b]	470	668	—	—	0.99	5250	0.66 ± 0.02
Experiment	470	—	513.4	~ 0	1.02	4544	0.63
Experiment	725	—	491.0	~ 0	1.20	4389	1.79

[a] Kohn–Sham AIMD simulation by Kresse [2].
[b] Classical MD simulation with neutral pseudoatom (NPA) potentials by Canales *et al* [4].

A detailed account of the generation of the first of them, which will be referred to as pseudopotential A, is given in reference [20]. In short, this local pseudopotential was obtained in a three-stage 'inversion' procedure: (1) the Troullier–Martins method [23] was used to generate an *ab initio* non-local pseudopotential for a Li atom using a $1s^2 2s^1 p^0$ configuration. (2) The non-local pseudopotential was introduced into a Kohn–Sham calculation for a bcc crystal (two atoms) of Li at the melting point density of the system. (3) The electron density obtained in the KS crystal calculation is input into the OF program and, by requiring that the electronic energy functional is minimized by this density, we obtain the *local* pseudopotential that gives rise to the same valence electron density. The pseudopotentials obtained in this way gave good crystal properties for Li (and several other simple metals), including the phonon dispersion curves [20].

In view of the findings to be reported below, we note an important limitation of this procedure. Because the inversion (step 3) is carried out on the electron density of a crystal, the lowest wavevector at which the electron density is a non-vanishing Fourier coefficient is at the first Bragg peak ($\sim$2.5 Å^{-1}). Since the inversion procedure is linear in the Fourier coefficients of the density, this means that the Fourier coefficients of the pseudopotential for smaller wavevectors are undetermined. In practice, the $k = 0$ value is required to yield the same total energy in the OF calculation as the KS one and the pseudopotential is assumed to be of Gaussian shape at low k.

In order to cope with this drawback a second pseudopotential for Li (pseudopotential B) has been generated and tested. The approach applied to obtain this new pseudopotential is based on the solution of the electronic problem posed by an ion embedded in an electron gas. A considerable amount of effort [15, 24–26] has been devoted to this issue, whose main goal is the determination of the induced or 'screening' density $n(r)$ (departure from the average density of electrons) around the ion in its 'jellium' environment. González *et al* [15] *pseudized* $n(r)$ (calculated by means of the so-called *neutral pseudoatom method* [24]) and obtained a pseudopotential using linear response theory. That is, the pseudopotential is generated in such a way that, assuming linear response, it reproduces the pseudized $n(r)$ at a given thermodynamic state. In our new approach [27], we use instead the OF functional (which also includes non-linear effects) to carry out the same 'inversion' procedure as mentioned in the generation of the pseudopotential of type A, but using now as input the pseudized 'jellium' induced density $n(r)$. Since this screening density is calculated in an infinite system, there are no limitations in the use of low k-values. We have obtained $n(r)$ at the same jellium density as that of the valence electrons in the liquid at 470 K. The solution of the electronic structure problem for the atom in the electron gas was achieved through the 'jellium–vacancy' formalism of Chihara [26].

The generation of pseudopotential B is, therefore, an *ab initio* procedure, save that the average electron density of the target system is used as an input to the calculation.

Pseudopotentials A and B are plotted in figure 1. The most striking point is that the pseudopotential B shows a knee at a k-value close to $2k_f$, k_f being the Fermi wavevector at 470 K ($k_f = 0.580$ au^{-1}). For the reasons pointed out previously, this behaviour is missed in the construction of pseudopotential A ($2k_f$ corresponds roughly to the first Bragg k-vector) and, as we will see below, it proves crucial to describing correctly liquid lithium in the long-wavelength region.

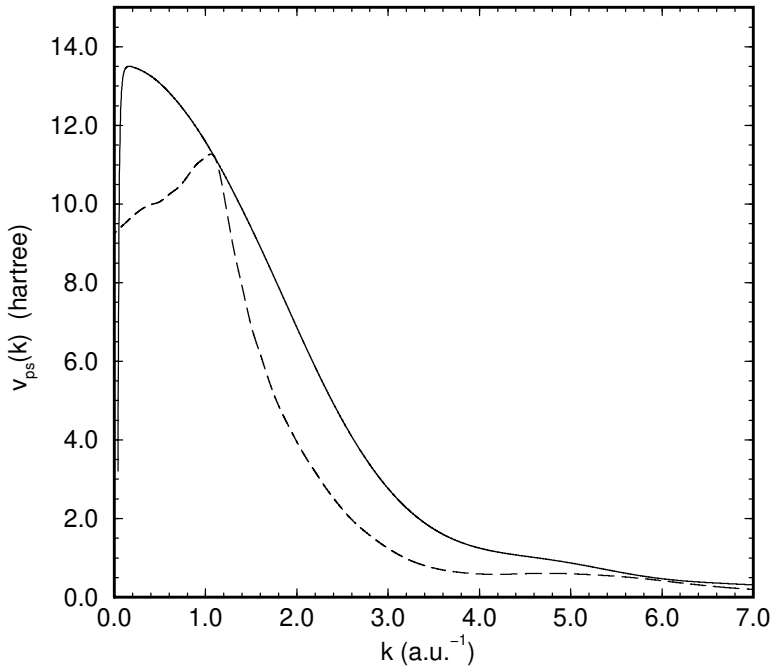

Figure 1. The non-Coulombic part of the pseudopotentials used in this work. Solid curve: pseudopotential A; dashed curve: pseudopotential B.

3. Static structure and ion–electron correlations

The ion–ion and ion–electron (partial) static structure factors of liquid Li were calculated throughout the simulation by averaging the instantaneous fluctuations of the ionic and valence electron densities via the usual Ashcroft–Langreth formula [1, 28]

$$S_{ij}(\boldsymbol{k}) = \frac{1}{\sqrt{N_i N_j}} \langle \rho_i(\boldsymbol{k}) \rho_j(-\boldsymbol{k}) \rangle \tag{1}$$

where $\rho_i(\boldsymbol{k})$ and $\rho_j(-\boldsymbol{k})$ are the Fourier components of the respective densities ($i, j = I, e$). In this way we have determined the ion–ion, $S_{II}(k)$, and ion–electron, $S_{Ie}(k)$, structure factors for all k-vectors compatible with the periodic boundary conditions. The distribution functions are then calculated by back Fourier transformation of the partial structure factors

$$g_{ij}(\boldsymbol{r}) = 1 + \frac{1}{\sqrt{\rho_i \rho_j}} \int \left[S_{ij}(\boldsymbol{k}) - \delta_{ij} \right] \mathrm{e}^{-\mathrm{i}\boldsymbol{k}\cdot\boldsymbol{r}} \, \mathrm{d}\boldsymbol{k} \tag{2}$$

or directly in real space, although this latter procedure is shown to give essentially the same results.

3.1. Ion–ion correlations

The results for $S_{II}(k)$ can be found in figure 2 (structure factors) and figure 3 (radial distribution functions). The theoretical predictions are seen to reproduce the experimental neutron structure factors [19] remarkably well, at the level of resolution seen in the main panel. Greater discrepancies can be seen with respect to the x-ray structure factor. To some extent this may be due to the fact that $S_{II}(k)$ is obtained from the experimental x-ray structure factor by assuming that the electronic form factor in the metal is the same as that for the isolated atom. The Li data will be particularly sensitive to errors in this approximation due to the high ratio of valence to core electrons [29]. For simulations performed with pseudopotential A, the results depart significantly from the experimental data only around the main peak and in the low-k region. With respect to the principal-peak region, we have discussed elsewhere [14] that there is a tendency in simulations with relatively small numbers of particles to overestimate the height of the main peak in liquid metals (where the density of the liquid is similar to that of the solid) because the periodic boundary conditions tend to induce a quasi-crystalline order [30]. For instance, the structure factor obtained in the KS-AIMD simulations by Kresse [2] shows a clear overestimation at the position of the main peak. Nevertheless, the results presented here prove to be very accurate when compared with the neutron structure factors, especially for pseudopotential B. This may be a consequence of the long times spanned by the simulations, for which a better equilibration of the sample could be achieved.

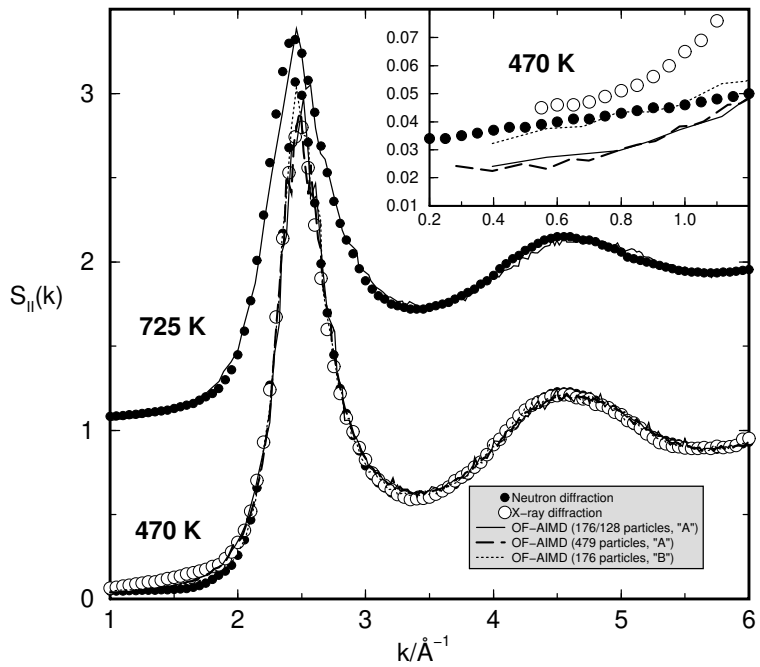

Figure 2. The ion–ion static structure factor of liquid Li. The results at the higher temperature are shown displaced upwards by unity. Diffraction data are taken from reference [19].

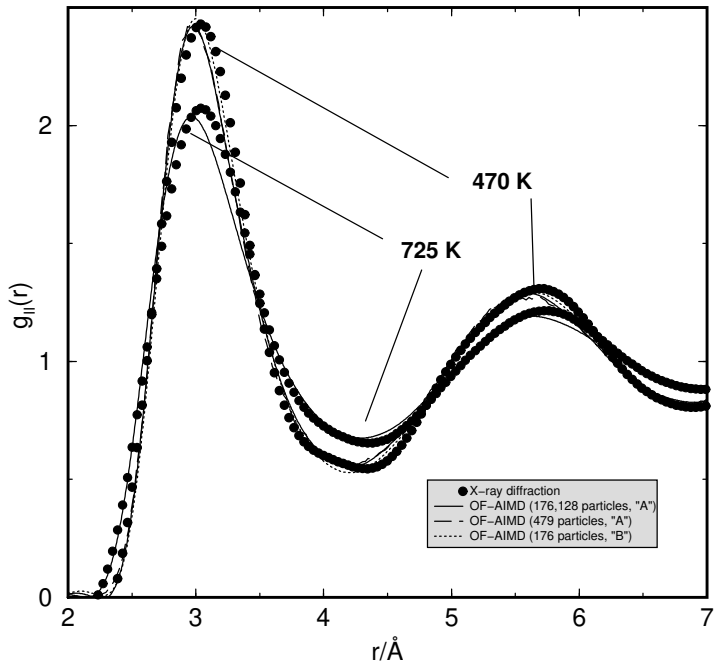

Figure 3. Ion–ion radial distribution functions of liquid Li; experimental data from reference [19].

At low wavevectors the OF-AIMD results with pseudopotential A lie systematically below the experimental data (inset to figure 2). This is not due to system size effects, as the 176- and 479-particle simulations give similar results in the common accessible k-range. On the other hand, the simulation with pseudopotential B seems to give the correct low-k behaviour. In addition, we have estimated the value of the compressibility χ_T ($=S_{II}(0)/\rho k_B T$) by fitting the simulation data at small wavevectors to a second-order polynomial and extrapolating to $k = 0$ (see table 1). The simulation with pseudopotential B gives a better estimate of the compressibility for the same number of particles. We therefore believe that the new pseudopotential generation method, which allows for the direct determination of the potential at low k, is the method of choice for constructing local pseudopotentials for orbital-free calculations.

Turning to real-space properties, excellent agreement is observed in the radial distribution function at 470 K (see figure 3), showing that the *ab initio* calculation describes correctly the local structure of ions. At the higher temperature, the agreement is somewhat poorer, probably because of the lack of transferability of pseudopotential A, the only one used at 725 K.

3.2. Electron–ion correlations

For the reasons pointed out in the introduction, the analysis of the results for the ion–electron structure factor $S_{Ie}(k)$ deserves particular attention. As shown in a previous paper [14] the relation between x-ray and neutron diffraction structure factors is given by

$$S_X(k) = \frac{[f_I(k) + \tilde{n}(k)]^2}{f_A^2(k)} S_N(k). \tag{3}$$

where $f_I(k)$ and $f_A(k)$ are, respectively, the ionic and atomic form factors, $S_X(k)$ and $S_N(k)$ ($=S_{II}(k)$) are the coherent x-ray and neutron diffraction structure factors, and $\tilde{n}(k)$ is the effective *'screening' density* in Fourier space in the liquid, i.e., the average density of

valence electrons that surrounds each ion in the liquid relative to the uniform background (in other words: the form factor of the *pseudoatom*). To obtain the coherent scattering from the total scattering requires the removal of an incoherent background whose exact form is still under discussion in the x-ray case [19, 21]. Given the x-ray and neutron diffraction experimental structure factors, and the experimental ionic form factor, $\tilde{n}(k)$ may be obtained from equation (3). The experimental ion–electron structure factor $S_{Ie}(k)$ is then simply given by [14]

$$S_{Ie}(k) = \frac{1}{\sqrt{z}}\tilde{n}(k)S_{II}(k) \tag{4}$$

where z is the ionic charge, and this may be compared with the simulation ion–electron structure factor obtained from (1). Extraction of $\tilde{n}(k)$ from the experimental data involves taking the ratio of $S_X(k)$ and $S_N(k)$ and then subtracting $f_I(k)$: if $\tilde{n}(k)$ is small compared to $f_I(k)$, which is the case for most elements of appreciable atomic numbers, this places a very high demand on the precision of the x-ray and neutron measurements. This procedure is equivalent to that used by Takeda *et al* [22] to extract the ion–electron structure factors for Na, Mg and Al, for which, in a previous paper [14], we found a qualitative disagreement between calculated and experimental quantities. The interesting point about Li is that the ratio of valence to core electrons is very high. Since it is precisely the deviation of $\tilde{n}(k)$ with respect to the valence electron distribution of an isolated atom from which the differences between x-ray and neutron scattering arise, we could expect that the procedure of extracting the ion–electron structure factor from experiment would be more accurate in the Li case.

We have then used the neutron and x-ray diffraction structure factors of Olbrich *et al* [19] to obtain the ion–electron structure factor. The result is displayed in figure 4 together with

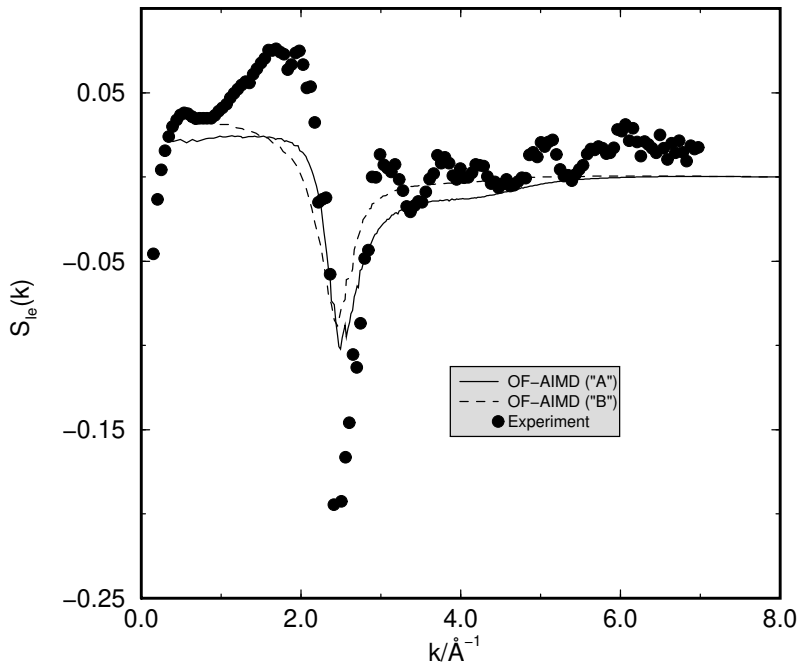

Figure 4. The ion–electron partial structure factor of liquid Li at 470 K; experimental data extracted from reference [19] in this work.

$S_{Ie}(k)$ obtained from the simulation. Appreciable deviations can be observed, especially in the region of the main peak and at high k. The rapid oscillations at high k and the shape of the function in the region of the first peak of the experimental data seem to be consistent with a difference in the resolution of the neutron and x-ray experiments. However, the magnitude of the calculated and experimental structure factors is closer than obtained for the heavier elements studied previously.

Unlike the ion–ion structure factors, the ion–electron correlations are seen to be very sensitive to the choice of pseudopotential, and again the pseudopotential B seems to give the correct low-k behaviour (where any experimental resolution problem should be less pronounced because of the slow k-dependence of the structure factor in this region). The effect of the pseudopotential is also visible in the ion–electron radial distribution functions (see figure 5), which were obtained from back Fourier transformation of the theoretical $S_{Ie}(k)$. As is well known, the first dip of $g_{Ie}(r)$ is correlated to the first maximum of $g_{II}(r)$. From the comparison of the functions at two different temperatures, it can be seen that an increase of the temperature (or a lowering of the density) causes the valence electrons to be more tightly localized around the ions.

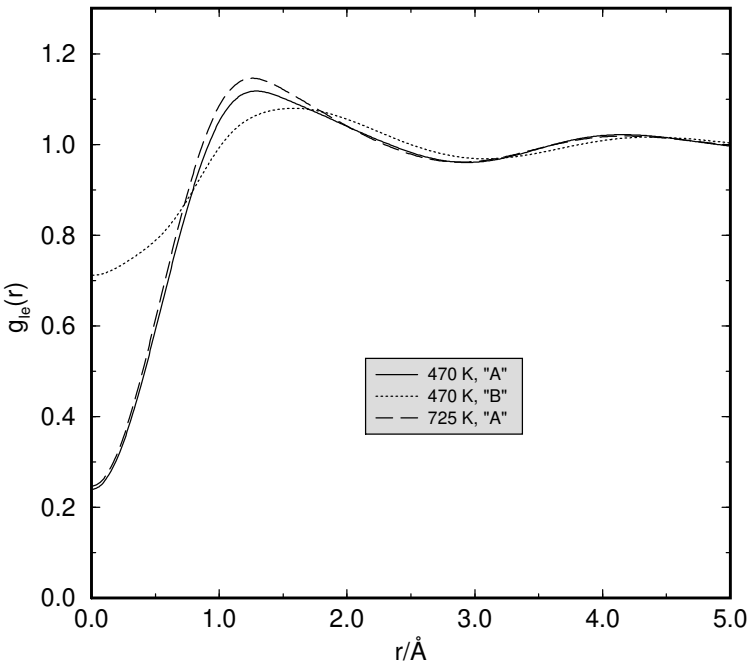

Figure 5. The calculated ion–electron radial distribution functions of liquid Li.

4. Dynamic properties

The dynamic structure factor $S(k, \omega)$ of Li at 470 K (figures 6 and 7) has been obtained from a direct Fourier transformation in time of the intermediate scattering function $F(k, t)$ which is defined as

$$F(k,t) = \frac{1}{N}\langle \rho_I(\boldsymbol{k}, t + t_0)\rho_I(\boldsymbol{k}, t_0)\rangle. \tag{5}$$

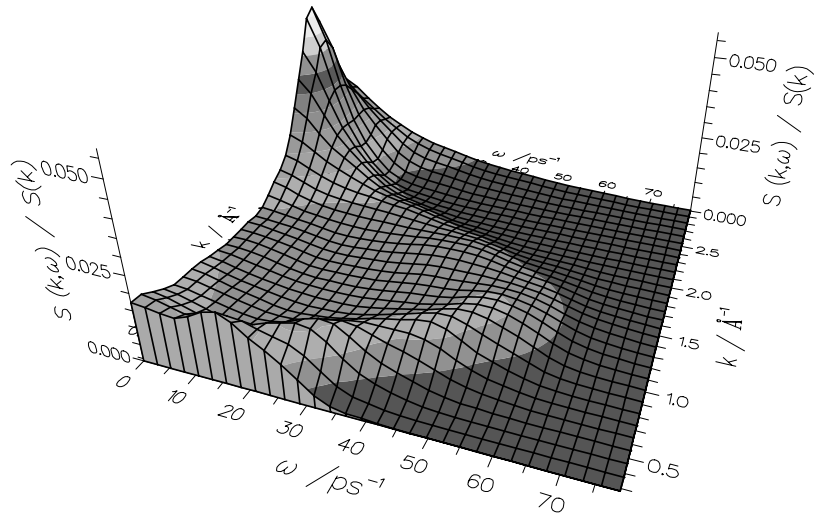

Figure 6. The dynamic structure factor or liquid Li at 470 K as obtained from OF-AIMD simulation with 479 particles. Note: this particular representation corresponds to the pseudopotential A.

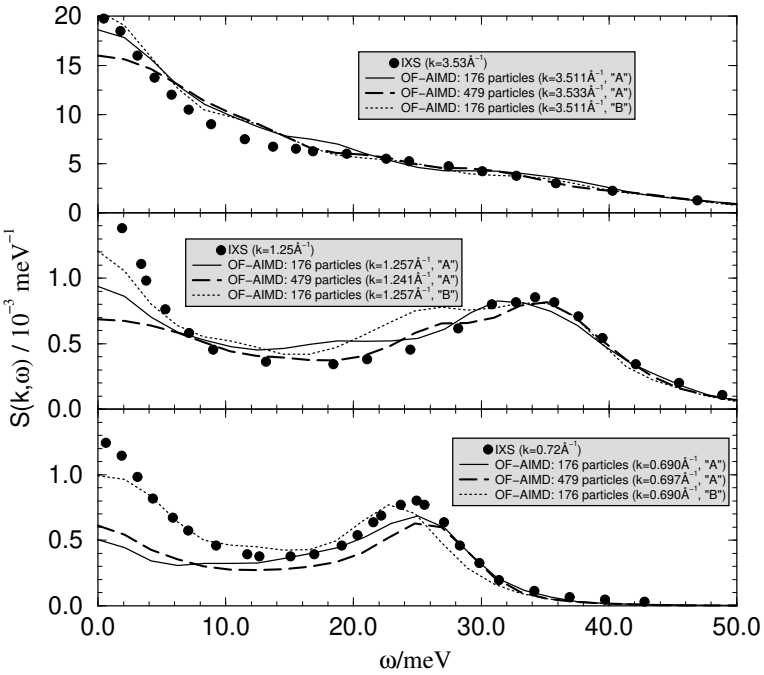

Figure 7. Comparison of the theoretical dynamic structure factor at three different wavevectors with inelastic x-ray scattering (IXS) results [17].

To perform the time average $\langle \cdots \rangle$ occurring in equation (5) we have sampled the ion positions every 50 steps. A maximum correlation time $t = 1$ ps was used and a Blackman window [31] was used to diminish the effect of the truncation in the Fourier transformation, giving a

resolution in the frequency domain of around 3 ps^{-1}.

As can be seen in figure 6, a Brillouin peak persists up to $k \sim 2$ $Å^{-1}$, i.e., very close to the position of the principal peak in the static structure factor (see figure 2). This shows that the liquid supports collective excitations for wavelengths comparable with the mean inter-particle spacing, a distinctive and well-known characteristic of liquid metals [1, 28].

In figure 7 the theoretical and the experimental (inelastic x-ray) dynamic structure factors [17] are displayed. The comparison is absolute, i.e. there has been no shift of the vertical or horizontal scale. Excellent agreement is found at higher k for all cases. At lower k the simulations correctly predict the appearance of a Brillouin peak, and the calculated Brillouin shift and width are in good agreement with experiment. In addition to the Brillouin peak at ∼35 meV, the data at 1.25 $Å^{-1}$ show an additional peak at ∼27 meV which appears to be due to truncation errors in the Fourier transform. That the simulation with pseudopotential B seems to miss the experimental Brillouin peak in the lowest panel of the figure is due to the fact that the k-vector of the simulation (0.69 $Å^{-1}$) is shifted with respect to the experimental one (0.72 $Å^{-1}$) with which it is compared. In fact, pseudopotential B leads to a slightly better prediction of the sound speed, as we will see below. The calculated and experimental peak positions are compared in figure 8. The inelastic x-ray scattering measurements of Sinn *et al* [17] showed that the dispersion relation of the Brillouin mode is steeper than the slope that corresponds to the macroscopic sound speed. Thus, the system does not seem to reach the hydrodynamic limit until wavevectors around 0.4 $Å^{-1}$. This suggests that the best way to estimate the macroscopic sound speed c_s of liquid Li from the simulation is from the position of the Brillouin peak in $S(k, \omega)$ at the smallest wavevector accessible ($c_s = \omega_{max}/k$). Taking the slope of the dispersion relation at low k leads to a significantly higher sound speed, in

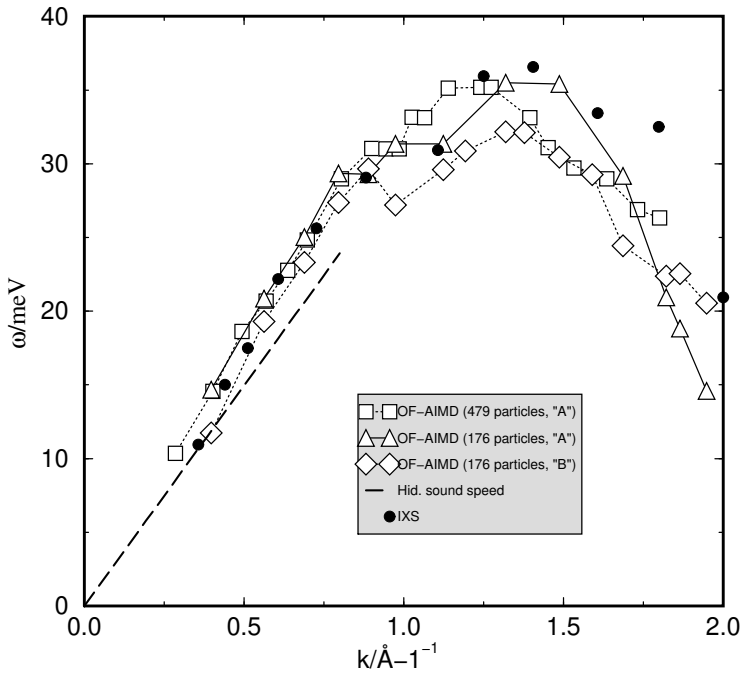

Figure 8. The dispersion relation of the Brillouin mode. IXS stands for inelastic x-ray scattering measurements [17].

accordance with the non-hydrodynamic behaviour observed in the experiment. The results for c_s using the first wavevector (see table 1) show that the best prediction of the macroscopic sound speed is obtained with pseudopotential B. This is not surprising bearing in mind that this pseudopotential is the one which gives a good compressibility.

Simulations with pseudopotential A appear to underestimate the intensity of the elastic line at low k, and to overestimate its width. This is not a system size artifact, as the results for 176 and 479 particles agree well. It is consistent with the aforementioned discrepancy between the calculated and experimental static structure factor at intermediate k for this pseudopotential. The frequency integral of the dynamic structure factor should equal the static structure factor and, as can be seen from the figure, the integral of the calculated data at $k \sim 0.72$ Å^{-1} is lower than in the experimental case by a factor which corresponds closely the underestimate of the static data at this value of k. In contrast, the simulation with pseudopotential B leads to a better dynamic structure factor in the low-frequency and low-wavevector region.

We have also calculated from the simulation data the mean square displacement $x^2(t)$ and the velocity autocorrelation function $C_{vv}(t)$, which are defined, respectively, as

$$C_{vv}(t) = \frac{\langle v_x(t)v_x(0)\rangle}{\langle v_x(0)^2\rangle} \tag{6}$$

$$x^2(t) = \langle |x(t) - x(0)|^2\rangle \tag{7}$$

where the time average $\langle\cdots\rangle$ has been calculated in the same manner as described before. The mean square displacements, as well as their time derivatives, are displayed in figure 9. It is observed that the relaxation time of the ionic velocities lies around 0.5 ps. The diffusion coefficient D can be calculated from these either by integration of $C_{vv}(t)$ (the Green–Kubo

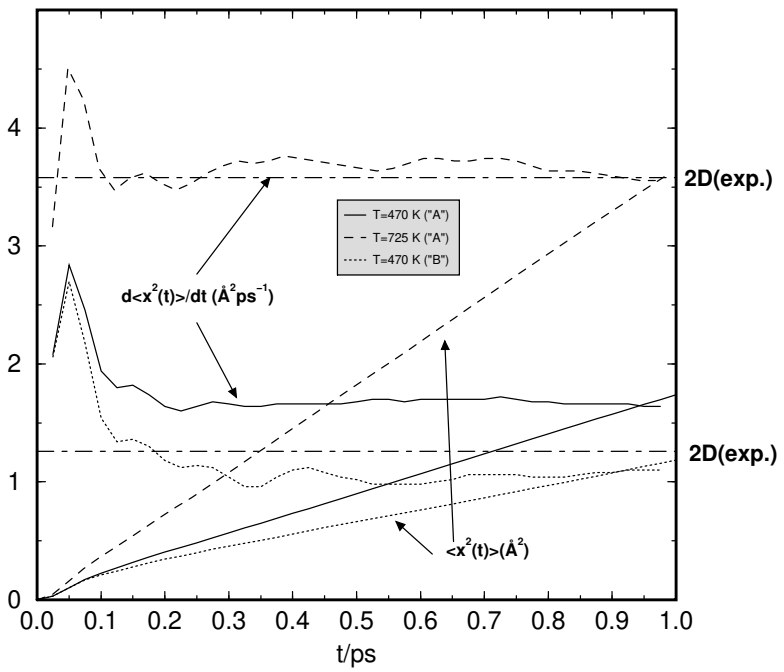

Figure 9. Mean square displacements (and their time derivatives) as computed from OF-AIMD simulation.

relation) or by differentiation of $x^2(t)$ (the Einstein relation)

$$D = \frac{k_B T}{M} \int_0^\infty C_{vv}(t)\, \mathrm{d}t \tag{8}$$

$$D = \frac{1}{2} \lim_{t\to\infty} \frac{\mathrm{d}x^2(t)}{\mathrm{d}t}. \tag{9}$$

The results for the diffusion coefficient are collected in table 1. Figure 9 also shows the time derivative occurring in the right-hand side of equation (9). Again the simulation with pseudopotential B provides a better estimate of the diffusion coefficient, although this turns out to be slightly smaller than that from the experiment.

5. Conclusions

By the standards of most simulation studies, the quality of the agreement between the calculated and experimental static figure 2 and dynamic figure 7 structure factors is extremely good. Particularly high standards have been set in the case of Li, by the high quality of the experimental data. The quality of these data has driven us to revise our previously published method of pseudopotential generation. The new pseudopotential and the OF-AIMD method give an excellent representation of lithium, which is always regarded as a difficult case because of non-locality. The only empirical information used in the calculations is the experimental density and, even here, the simulation pressure is very small, so working at zero pressure would have had little effect on the results. The simulations used modest computational resources, and there is considerable scope for achieving further increases in efficiency for larger system sizes by using e.g. multiple-time-step methods [32].

As regards the ion–electron structure factor, we have seen that the theoretical predictions for this quantity in Li do not show a much better accord with the currently available experimental data than was the case for Na, Mg and Al. There are still discrepancies which suggest that a better treatment of the corrections in both neutron and x-ray scattering measurements should be applied.

Acknowledgments

JAA thanks the Ministerio de Educación y Cultura of Spain for the award of a postdoctoral fellowship. The work was supported by EPSRC grant GR/L49369 and by the UKCP consortium. Some of the calculations were carried out at the Oxford Supercomputing Centre. We are grateful to Philip Salmon for discussions on the extraction of the electron–ion structure factor from experimental data.

References

[1] Hafner J 1987 *From Hamiltonians to Phase Diagrams* (Berlin: Springer)
[2] Kresse G 1996 *J. Non-Cryst. Solids* **205–207** 833
[3] Kambayashi S, Nowotny G, Chihara J and Kahl G 1996 *J. Non-Cryst. Solids* **205–207** 914
[4] Canales M, González L E and Padró J A 1994 *Phys. Rev.* E **50** 3657
Canales M, Padró J A, González L E and Giró A 1993 *J. Phys.: Condens. Matter* **5** 3095
[5] de Wijs G A, Pastore G, Selloni A and van der Lugt W 1995 *Phys. Rev. Lett.* **75** 4480
[6] Car R and Parrinello M 1989 *Phys. Rev. Lett.* **55** 2471
[7] Remler D K and Madden P A 1990 *Mol. Phys.* **70** 921
[8] Payne M C, Teter M P, Allan D C, Arias T A and Joannopoulos J D 1992 *Rev. Mod. Phys.* **64** 1045
[9] Parr R G and Yang W 1989 *Density-Functional Theory of Atoms and Molecules* (Oxford: Oxford University Press)

[10] Pearson M, Smargiassi E and Madden P A 1993 *J. Phys.: Condens. Matter* **5** 3221
[11] Smargiassi E and Madden P A 1994 *Phys. Rev.* B **49** 5220
[12] Foley M, Smargiassi E and Madden P A 1994 *J. Phys.: Condens. Matter* **6** 5231
[13] Foley M and Madden P A 1996 *Phys. Rev.* B **53** 10 589
[14] Anta J A, Jesson B J and Madden P A 1998 *Phys. Rev.* B **58** 6124
[15] González L E, González D J, Silbert M and Alonso J A 1993 *J. Phys.: Condens. Matter* **5** 4283
[16] de Jong P H K, Verkerk P and de Graaf L A 1966 *J. Non-Cryst. Solids* **156–158** 48
[17] Sinn H, Sette F, Bergmann U, Halcoussis Ch, Krisch M, Verbeni R and Burkel E 1997 *Phys. Rev. Lett.* **78** 1715
[18] Ohse R W (ed) 1985 *Handbook of Thermodynamic and Transport Properties of Alkali Metals* (Oxford: Blackwell)
[19] Olbrich H, Ruppersberg H and Steeb S 1983 *Z. Naturf.* a **38** 1328
[20] Watson S, Jesson B J, Carter E A and Madden P A 1998 *Europhys. Lett.* **41** 37
[21] Chihara J 1987 *J. Phys. F: Met. Phys.* **17** 295
[22] Takeda S, Kawakita Y, Inui M, Maruyama K, Tamaki S and Waseda Y 1996 *J. Non-Cryst. Solids* **205–207** 365
[23] Troullier N and Martins J L 1991 *Phys. Rev.* B **43** 1993
[24] Dagens L 1972 *J. Phys. C: Solid State Phys.* **5** 2333
[25] Manninen M, Jena P, Nieminen R M and Lee J K 1981 *Phys. Rev.* B **24** 7057
[26] Chihara J 1989 *Phys. Rev.* A **40** 4507
[27] Anta J A, Jesson B J and Madden P A 1999 to be published
[28] Hansen J-P and McDonald I R 1986 *Theory of Simple Liquids* (New York: Academic)
[29] Anta J A and Louis A A 1999 to be published
[30] Denton A R and Egelstaff P A 1997 *J. Phys. B: At. Mol. Phys.* **103** 343
[31] Allen M P and Tildesley D J 1987 *Computer Simulation of Liquids* (Oxford: Clarendon)
[32] Tuckerman M E and Parrinello M 1994 *J. Chem. Phys.* **101** 1316